Pharm Res (2010) 27:1659–1676
DOI 10.1007/s11095-010-0166-y

RESEARCH PAPER

Development of New Localized Drug Delivery System Based on Ceftriaxone-Sulbactam Composite Drug Impregnated Porous Hydroxyapatite: A Systematic Approach for *In Vitro* and *In Vivo* Animal Trial

Biswanath Kundu • Chidambaram Soundrapandian • Samit K. Nandi • Prasenjit Mukherjee • Nandadulal Dandapat • Subhasis Roy • Bakul K. Datta • Tapan K. Mandal • Debabrata Basu • Rupnarayan N. Bhattacharya

Received: 1 February 2010 / Accepted: 22 April 2010 / Published online: 13 May 2010

ABSTRACT

Purpose Present investigation deals with an extensive approach incorporating *in vitro* and *in vivo* experimentation to treat chronic osteomyelitis, using hydroxyapatite porous scaffolds.

Materials and Methods Hydroxyapatite was synthesized in the laboratory by wet chemical method, different porous scaffolds have been fabricated. *In vitro* studies include variation of porosity with interconnectivity, pore-drug interfacial studies by SEM-EDAX and drug elution studies (by HPLC) both in contact with PBS and SBF at ~37°C. *In vivo* trials were based on experimental osteomyelitis in rabbit model induced in tibia by Staphylococcus aureus. Characterizations included observation of histopathology, radiology and estimation of drug in both bone and serum for 42 days by HPLC method and subsequent bone-biomaterial interface by SEM.

Results It was established that lower pore percentage with a distribution of mainly micro-pores were found to be superior over the higher pore percentage both *in vitro* and *in vivo*. The criteria was matched with the 50N50H samples which had 50–55% porosity with an average pore size ~110 μm, having higher interconnectivity (10–100 μm), moderately high adsorption efficiency (~50%) when loaded with CFS (drug combinations consisting of irreversible b-lactamase inhibitor and b-lactam antibiotic). CFS release from HAp implants were faster in PBS than SBF. Further, both the results of *in vitro* and *in vivo* drug elution after 42 days showed release higher than minimum inhibitory concentration of CFS against Staphylococcus aureus. *In vivo* studies also proved the superiority of CFS loaded HAp implants than parenteral group based on eradication of infection and new bone formation.

B. Kundu • C. Soundrapandian • N. Dandapat • D. Basu
Bioceramics and Coating Division,
Central Glass and Ceramic Research Institute,
Kolkata, India

B. Kundu
e-mail: biswa_kundu@rediffmail.com

C. Soundrapandian
e-mail: soundr@rediffmail.com

N. Dandapat
e-mail: nanda_dandapat@yahoo.co.in

D. Basu
e-mail: dbasu@cgcri.res.in

S. K. Nandi (✉) • P. Mukherjee • S. Roy
Department of Veterinary Surgery and Radiology,
West Bengal University of Animal and Fishery Sciences,
Kolkata, India
e-mail: samitnandi1967@gmail.com

P. Mukherjee
e-mail: vetprasenjit@gmail.com

S. Roy
e-mail: subhasisvet@yahoo.co.in

B. K. Datta • T. K. Mandal
Department of Veterinary Pharmacology and Toxicology,
West Bengal University of Animal and Fishery Sciences,
Kolkata, India

B. K. Datta
e-mail: drbkd75@gmail.com

T. K. Mandal
e-mail: drtkm48@yahoo.co.in

R. N. Bhattacharya
Department of Plastic Surgery,
R.G. Kar Medical College and Hospital,
Kolkata, India
e-mail: rupnarayan.bhattacharya@gmail.com

Conclusions HAp based porous scaffold loaded with CFS and designed porosity (in terms of micro- and macro-porosity, interconnectivity) was found to be an ideal delivery system which could locally, sustainably release the composite antibiotic in reliable manner both in terms of *in vitro* drug elution behaviour in contact with SBF and *in vivo* animal trial.

KEY WORDS ceftriaxone-sulbactam composite · *in vivo* animal trial · osteomyelitis and new bone formation · porous hydroxyapatite · SBF

ABBREVIATIONS

ASTM	American Society for Testing and Materials
AUC	Area under the curve
CFA	Colony-forming unit
CFS	Combination of CFT and SUL drug
CFT	Ceftriaxone sodium
FESEM	Field emission scanning electron microscopy
FTIR	Fourier-transformed infrared spectroscopy
HAp	Hydroxyapatite
HPLC	High performance liquid chromatography
MIC	Minimum inhibitory concentration
PBS	Phosphate buffered saline
PMMA	Poly-methyl methacrylate
RBC	Red blood cell
SBF	Simulated body fluid
SEM-EDAX	Scanning electron microscopy-Energy dispersive analysis of X-ray
SUL	Sulbactam sodium
XRD	X-ray diffraction

INTRODUCTION

The treatment of acute and chronic orthopaedic infections is difficult, time-consuming and expensive (1). As the condition is frequently associated with poor vascular perfusion accompanied by infection of surrounding tissue (2), surgical debridement and prolonged administration (about 4–6 weeks) of antibacterial agents constitute the mainstay therapy for orthopaedic infections (3). Despite the availability of a myriad of antibiotics and marked advances in surgical treatment, the long-term recurrence rate remains alarming at a rate of 20% to 30% (4). Absence of antibiotics labelled exclusively for osteomyelitic conditions leave the choice of therapy to the preferences and experience of the attending physicians (5). Very high concentrations of antibiotics are required at the target site but could hardly be attained by conventional routes of drug administration without provoking serious side effects (6). Hence, conventional therapy hampers clinicians in striking a balance between efficacy and safety in deciding an optimal treatment strategy for osteomyelitic patients. On the other hand, patients feel frustrated at unfulfilled therapeutic outcomes and development of adverse drug effects, if any, in addition to weeks of stay in hospital and huge healthcare bills. Local drug delivery systems, when placed in the affected area, release drug locally for prolonged periods and at concentrations generally higher than those achieved by conventional drug delivery strategies. The low cost of therapy, better healing rate and insignificant chances for development of side effects or adverse drug effects are some impressive advantages of local drug delivery.

Different antibiotic loaded-local drug delivery systems for the treatment of osteomyelitis made of polymers as PMMA (synthetic polymer) (7,8), collagen (9) (natural polymer) were tried, but resulted in poor antibiotic elution properties (7,8) and insufficient duration of antibiotic release (9). New methods, such as local delivery of antibiotics with bone bioactive ceramics, have proved to improve the prognosis of orthopaedic infections (10,11). Among all bioceramic implantable delivery systems described in the literature, HAp, that constitutes the inorganic part of the bone, has added advantages in terms of biocompatibility, bioactivity and high binding affinity for a variety of bioactive molecules (12,13). Unlike polymers, bioceramic matrices such as HAp perform multiple functions, such as releasing bioactive molecules for prolonged period and aiding space filling for reconstruction and or regeneration of living tissues in the local area (14–16). However, before designing a porous scaffold, we need to consider the influence of pores in the constructs (17–20). Once the engineered construct is placed in the body, blood flow and vascularization become key issues for drug release and further remodelling in the *in vivo* environment. *In vivo* bone tissue ingrowth is affected by pore size, as it influences migration and proliferation of osteoblasts and mesenchymal cells and matrix deposition in the empty space (21,22) together with drug diffusion. Pore interconnection provides the channel for cell distribution and migration, allowing efficient blood vessel formation (23,24). These factors emphasize the importance of pore size, amount and interconnectivity in the scaffold. However, in the treatment of osteomyelitis, there are no reports on the effect of these variables on drug release from porous HAp scaffolds.

Bacteria are an excellent example of survival instincts and demonstrate unlimited capability to survive and evolve as new variants under adverse conditions. One of the classic survival strategies displayed by some pathogenic bacteria is the production of β-lactamases, an enzyme that inactivates β-lactam antibiotics. However, drug combinations that include an irreversible β-lactamase inhibitor with β-lactam antibiotics prove to be a rational counter-approach in the

treatment of infections caused by β-lactamase-producing strains (25,26). Such rational combinations decrease the MICs of hydrolyzed β-lactams to normal (27) and expand the antimicrobial spectrum to include previously β-lactam-resistant microorganisms (28). In this study, for the first time, sulbactam sodium (SUL), a β-lactamase inhibitor was evaluated in combination with ceftriaxone sodium (CFT), a β-lactam antibiotic in the treatment of osteomyelitis.

Finally, development of prolonged-release bioceramic porous scaffolds to treat orthopaedic conditions is at the juncture of three specialties: materials science, pharmaceutical science and medical science. Though considerable work has been reported earlier, a complete report from synthesis to animal trails justifying all the involved specialties is rare to locate.

To address the above concerns, our investigation was designed for a systematic and extensive research focused on: 1) development of highly interconnected porous HAp scaffold and in two variations of porosity, 2) development and detailed characterization of combined drug (CFT and β-lactamase inhibitor which can combat multiresistant pathogen) impregnated HAp porous scaffold, 3) *in vitro* drug delivery properties that include drug release efficiency in both PBS and SBF, and 4) *in vivo* animal trial to check the efficacy of select type of porous HAp scaffold loaded with novel drug combination (CFS) to combat chronic osteomyelitis and aid new bone formation.

MATERIALS AND METHODS

Synthesis and Characterization of Hydroxyapatite Powders

HAp powder was synthesized in the laboratory by a wet chemical method using analytical reagent-grade calcium hydroxide and ortho-phosphoric acid as the initial reactants with the Ca/P molar ratio of these two reactants maintained at ~1.67. Details of the procedures are outlined elsewhere (11,29). Thus, synthesized HAp powders except a part (as dried at 80°C) were calcined at 800°C and 1,250°C. Powders calcined at 800°C were used for fabrication of porous scaffolds, while powders calcined at 1,250°C were studied to assess the status of the powders in terms of phase composition, stability, crystallinity and average crystallite size so as to ascertain the sintering temperature to be applied in the process of porous scaffold formation. X-ray diffraction (XRD) (Philips Analytical B.V., X'Pert Pro, Netherlands) and Fourier transformed infra-red spectroscopy (FTIR) (Perkin-Elmer, Spectrum 100, USA) were taken for the as-dried (80°C) as well as the powders calcined at both 800° and 1,250°C. Degree of crystallinity (X_c) from XRD was calculated by using the following relationships (30):

$$X_C = 1 - \frac{V_{112/300}}{I_{300}}$$

where, I_{300} is the intensity of (300) plane reflection and $V_{112/300}$ is the intensity of the hollow between the planes (112) and (300) reflections.

Surface charge in terms of zeta potential of the powder (calcined powders fired at 1,250°) suspensions were also estimated for indirect estimation of interaction between these particles and CFS. Zeta potential of these particles was determined using suspensions containing 0.01%W/V of such particles in a 10^{-3} M KCl solution. The measurements were taken as a function of pH at 20°C. The pH was adjusted with 0.1 M KOH and 1 M HCl solutions for basic and acidic conditions, respectively.

Fabrication and Characterization of Porous Scaffolds

First, the powder calcined at 800°C was intimately mixed with appropriate quantity of naphthalene (SD Fine-Chem, India) powder by repeated sieving in a sieve shaker (Retsch, AS200, Germany). Porous units were fabricated by modification of a process earlier developed (31). In the present investigation, naphthalene was added at two different percentages of the scaffold formulation, viz., 50 and 60%, (hereinafter the same designated as 50N50H and 60N40H). The powder mix was subsequently compacted at a pressure of 150 MPa (for 40 s) by cold-isostatic pressing (EPSI N.V.; SO 10036, Belgium) to form cylindrical-shaped green specimens. Specimens having required dimensions suitable for further characterization were machined using a manual lathe machine. By heating up to 80°C, the naphthalene was driven off from the green specimens with care to prevent cracking at this stage. Finally, the green and now fragile specimens were sintered at 1,250°C for 2 h (heating rate 3°C/min. and air atmosphere). Physical properties including apparent or open porosity as well as bulk density of the sintered porous specimens were measured by Archimede's principle (ASTM C373-72).

Microstructure, pore size, shape and morphology were observed by field emission scanning electron microscopy (FESEM) (Carl Zeiss, Supra 35 VP, Germany) on one side of the flat-parallel surface. Image analysis was carried out to calculate the pore size distribution (Perfect Screen Ruler 2.0, Styopkin Software, USA). More than 250 linear measurements were taken from each micrograph and converted to their actual dimension from the corresponding tag of each microstructure. Histograms thus obtained were plotted as function of pore size ranges. The average pore sizes were also determined. The microstructures were mainly taken in back-scatter electron mode. Samples were mounted and sputter-

coated (Polaron, Quoram Technology, U.K.) with gold-palladium having a coating thickness ~6 nm to reduce charging and to improve the image quality prior testing.

Fabrication and Characterization of Drug Impregnated Scaffolds

We have used a combination of two drugs: CFT and SUL in 2:1 ratio. Five samples for each kind of porous scaffolds were soaked in a solution of CFS (500 mg/mL concentration) prepared in ultra-pure water (Milli-Q Academic Century, ZMQS50001, China) and subjected to a vacuum of 10 mmHg for at least 30 min. The samples were further freeze-dried (Eyela, FDU-2200, Japan) and checked for adsorption efficiency. This was expressed as percentage (the change in weight of HAp scaffold before and after drug impregnation work divided by the weight before impregnation).

A section of these CFS impregnated porous blocks was characterized for microstructural evolution using an SEM. Depending on the sample's composition, microstructures were taken either in secondary electron or back-scatter electron mode. The samples were mounted and, as before, sputter-coated with a thin film of carbon having a coating thickness ~10–20 nm to reduce charging and to improve the image quality prior to testing. For assessment of the compositional variation along the interface between pore surface and drug, EDAX was employed. The vacuum in the chamber was 1.14×10^{-6} mbar. Other parameters include beam current of electron gun: 1.0 nA, spot size: 520 nm, working distance: 8.5–9 mm, SiLi detector and collection time: 45 s. Depending on the microstructure observed, line-scan of EDAX was performed for compositional variation and compared with the said microstructure.

In vitro drug elution studies were performed in two liquid mediums: PBS and SBF. PBS used was a solution of salts as NaCl (137 mM), KCl (2.7 mM), Na_2HPO_4 (10 mM), KH_2PO_4 (1.8 mM) with a pH of 7.4, while SBF was prepared in accordance to Kokubo *et al.* with ionic concentrations equal to human blood plasma (32). CFS impregnated scaffolds were placed in test tubes containing 3 mL of liquid medium and stored in a thermostatic chamber at ~37.4°C. After each day up to 7 days and each week subsequently up to 42 days, the samples were removed and transferred to a new tube containing 3 mL of fresh liquid medium. The liquid mediums containing the released CFS were stored at −80°C until analysed. After filtration, the amount of CFT and SUL release were determined by HPLC (Shimadzu, SPD-MIOA, Japan) fitted with binary pump (LC-20 AT), diode array detector. Similar procedures were followed for obtaining the assays up to 42 days. The conditions for HPLC were as follows: for determination of CFT, the mobile phase was composed of HPLC grade water: acetic acid: acetonitrile ~70:5:25 with flow rate 1 mL/min. and detection wavelength 254 nm. The separation was carried out using an RPC_{18} pH stable column (Phase Separations, Norwalk, CT), 15 cm long. For determination of S, the mobile phase was a mixture of buffer: acetonitrile ~88:12 (the buffer was a solution of 0.1 M KH_2PO_4, tetra-butyl-ammonium hydroxide and 0.1 M phosphoric acid). The flow rate was 1.5 mL/min. with detection wavelength of 313 nm. Percent yield of CFS was expressed as the total amount of released antibiotic divided by the amount of CFS held in the samples before the start of elution in PBS and SBF separately.

In Vivo Studies

Bacterial Isolate

Staphylococcus aureus (coagulase positive) obtained from an animal infected with chronic osteomyelitis was used for development of experimental model in rabbit. Pure cultures of the bacteria were obtained on blood agar at 37°C and standardized suspensions (3×10^6 CFU/mL) prepared in saline. This sample (1 mL) was introduced into the medullary cavity of rabbit tibiae for successful induction of osteomyelitis by *Staphylococcus aureus* and the same confirmed by Manitol salt agar test.

Study Model

Animal experimentations were carried out following the procedures conforming to the Standards of the Institutions Animal Ethical Committee of the West Bengal University of Animal and Fishery Sciences, India. Osteomyelitis was induced in the right tibia of 24 New Zealand white rabbits (2.5–3 kg body weight) according to the model of Norden (33). The proximal part of the tibia was exposed anteriorly after anaesthesia with Nembutal 0.5 mg/kg intra venous (IV) (Thiopentone sodium, Thiosol®, Neonlab, Mumbai, India), and a hole was drilled through the cortex into the medullary cavity using a 1.2 mm diameter dental burr. One mL of *Staphylococcus aureus* suspension containing approximately 3×10^6 CFU/mL was injected into the drilled medullary cavity, and the hole was sealed with bone wax to prevent bacterial leakage into the surrounding soft tissues. The animals were monitored after surgery. All the animals received standard postoperative pain medication (Carprofen; 4 mg/kg of body weight) for 3 days. Only the animals who developed osteomyelitis after three weeks of inoculation were considered for the present study. CFS-impregnated HAp scaffolds (samples from 50N50H series) were implanted in the infected bone

and same postoperative management was followed. The 24 animals were divided into 3 groups: Group I, II and III. The details of the experimentation model with these animals are tabulated (Table I). All the samples required for the study parameters were obtained on 12, 21 and 42 days post osteomyelitis. Thoroughly washed 3–4 mm thick sections of implanted bone/antibiotic-impregnated HAp implants were fixed in 10% formalin for 7 days and subsequently decalcified in Goodling and Stewart's fluid-containing formic acid 15 ml, formalin 5 ml and distilled water 80 ml solution. Haematoxylin and eosin-stained decalcified cross-sections were considered for histological examinations. Radiographic images of the subjected bones were taken under direct radiographic magnification. Blood samples from the ear vein and pulverized, homogenized, centrifuged supernatant fluid from cortico-cancellous portion of tibia (removing bone marrow) were collected for estimation of antibiotic (CFT and SUL) by HPLC techniques by the methods described earlier. The results were expressed as means ± standard deviations.

Specimens were also collected for SEM analysis from the cortical part of the bone of animals from all the three groups after 42 days, while from Group II, samples were also collected after 21 days, post-operatively. For SEM specimens, 5% glutaraldehyde phosphate solution was used for fixing the samples, washed twice for 30 min. with PBS (pH 7.4) and distilled water, dehydrated in a series of graded ethanol followed by final drying with hexamethyldisilizane (HMDS). A gold conductive coating was given by ion sputtering (JEOL ion sputter, Model JFC 1100, Japan) at 7–10 mA and 1–2 kV for 5 min. The resin-mounted sample surfaces were then examined under SEM (JEOL JSM 5200 model, Japan) after proper alignment.

RESULTS

Powder Characterization

XRD of the powders prepared at 80°C and powders calcined at 800°C and 1,250°C are presented in Fig. 1 along with the standard. 800°C calcined powders were used to fabricate the porous blocks. It was found that the patterns were well matched with the standards in JCPDS PDF (Joint Committee on Powder Diffraction Standards Powder Diffraction Files) no. 09-0432, which corresponds to the phase HAp. Polycrystalline nature and purity of HAp phase were retained up to 1,250°C. These parameters were important for the study of drug impregnation subsequently.

X_c, which is the direct evidence of the amorphous content in the fabricated materials, was increased from 67.6% to 98.3% when the powders fired from 80° to 1,250°C. It was calculated to about 87.7% when the powders fired at 800°C.

FTIR spectrum of as-dried and powders fired at different temperatures are plotted together in Fig. 2. The band assignments of FTIR spectrum obtained at different wave numbers are summarized in Table II. It was evident that the respective functional groups for PO_4^{3-} and OH^- corresponding to HAp crystals (34,35) were present in Figs. 2a–c. However, band positions of OH^- at 3,580 and 630 cm^{-1} were absent in Fig. 2a. A very small hump at the wave number 1,454 cm^{-1} in this figure arose from vibrations of CO_3^{2-} ions. This effect was more pronounced in 800°C calcined powders (where there was another hump at 1,414 cm^{-1}) (Fig. 2b). At 1,250°C, however, carbonate peaks became insignificant. Bands at 3,454 and 1,615 cm^{-1} arose from adsorbed molecular water. The bands at 1,454 and 1,414 cm^{-1} attributed to CO_3^{2-} groups in the apatite structure are well defined (36,37). In Fig. 2a, the carbonate

Table I Design of Experiment for *In Vivo* Animal Experimentation

Groups	No. of animals	Implant	Days of experiment	Experiment
Group I	6	No implants	After 3 weeks	Six animals were sacrificed for histological, radiographic and microbiological examination to confirm development of osteomyelitis.
Group II	9	CFS injection parenterally (15 mg/kg bid) twice daily for 6 weeks	12 days	Three animals were sacrificed for histological and estimation of drug concentration in bone and serum.
			After 3 weeks	Three animals were sacrificed for histological and estimation of drug concentration in bone and serum
			After 6 weeks	Three animals were sacrificed for histological and estimation of drug concentration in bone and serum
Group III	9	CFS impregnated HAp scaffolds	12 days	Three animals were sacrificed for histological and estimation of drug concentration in bone and serum.
			After 3 weeks	Three animals were sacrificed for histological and estimation of drug concentration in bone and serum.
			After 6 weeks	Three animals were sacrificed for histological, radiographic, and estimation of drug concentration in bone and serum.

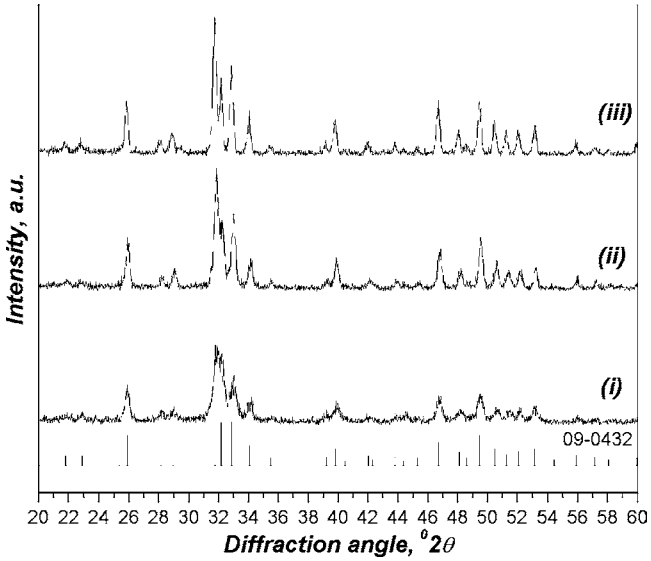

Fig. 1 X-ray diffraction of the powder synthesized by wet chemical method; (*i*) as-dried (80°C); calcined at (*ii*) 800°C and (*iii*) 1,250°C.

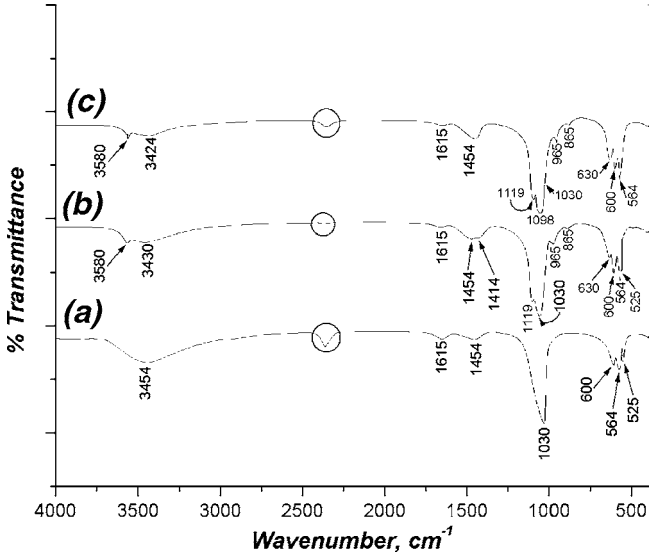

Fig. 2 FTIR spectrum of the powder synthesized by wet chemical method; (**a**) as-dried (80°C); calcined at (**b**) 800°C and (**c**) 1,250°C.

band at 1,454 cm^{-1} corresponds to incorporation of CO_3^{2-} groups at the OH^- position (A-type) and the same band at 1,414 cm^{-1} (Fig. 2b) to the occupation of PO_4^{3-} sites in the apatite structure (B-type). The band at 865 cm^{-1} was assigned to both types of incorporation (Narasaraju and Phebe, 1996, Suetsugu *et al.*, 1998). At 1,250°C, the intensity of the bands both at 1,454 and 1,414 cm^{-1} was decreased (Fig. 2c). This could be interpreted as a release of carbonate from PO_4^{3-} positions in the apatite structure.

Characterization of Porous Scaffolds

Physical parameters such as percent open porosity and bulk density of the porous HAp scaffolds measured by Archimedes' water displacement method are given in Table III.

Table II Band Assignments of IR Spectrum Given in Fig. 2

Wavenumber, cm^{-1}	Assignment/s
3,700–3,000	H–O–H, Water of crystallization or adsorbed water
3,580	O–H, (OH) group
1,615	H–O–H, Water of crystallization or adsorbed water
1,454, 1,414	C–O of CO_3 groups
1,119, 1,098	P–O and P–OH, HPO_4, and PO_4 groups
1,030	P–O in HPO_4, and PO_4 groups (stretching mode)
965	P–O in PO_4 group
865	P–OH stretching mode of HPO_4 groups
630	O–H of OH group
600, 564	P–O in PO_4 groups (bending mode)
525	HO–PO_3 bending mode in HPO_4

It was found that the increase in naphthalene content in the formulation resulted in higher porosity and hence lesser bulk density in 60N40H samples as expected. Further, increase of naphthalene by 10% resulted in increase of open porosity by 10%. SEM microstructures of the porous body fabricated using different percentage of naphthalene (50N50H and 60N40H) are presented in Figs. 3a and b. Histograms based on image analysis were plotted as function of pore size ranges and are presented in Fig. 4 for 50N50H and 60N40H samples. The microstructures were very non-uniform with high interconnectivity of pores. A bimodal distribution of pores was seen for the 60N40H samples. Macropores (>50 μm) were mainly evidenced from both the micrographs and with lesser amount of micropores in 60N40H samples than the 50N50H one. The average pore size for both kinds of samples was calculated and found to be ~114.3 and 140.2 μm for 50N50H and 60N40H samples, respectively. It was noticed that with increasing amount of naphthalene, the spherical nature of pore shapes (when the naphthalene percentage was only ~5–10%) started to change, and the void shapes were ruptured (when the naphthalene percentage was ~30%). More and more non-uniform release of this fugitive material was evident as were the microstructures of 50N50H and 60N40H samples. However, superior inter-

Table III Physical Properties of Porous Scaffolds Used for Subsequent Fabrication of Drug Delivery System

Sample	Bulk density, g/c.c.	Apparent porosity,%
50N50H	1.47 ± 0.05	53.61 ± 2.14
60N40H	1.11 ± 0.05	64.46 ± 3.22

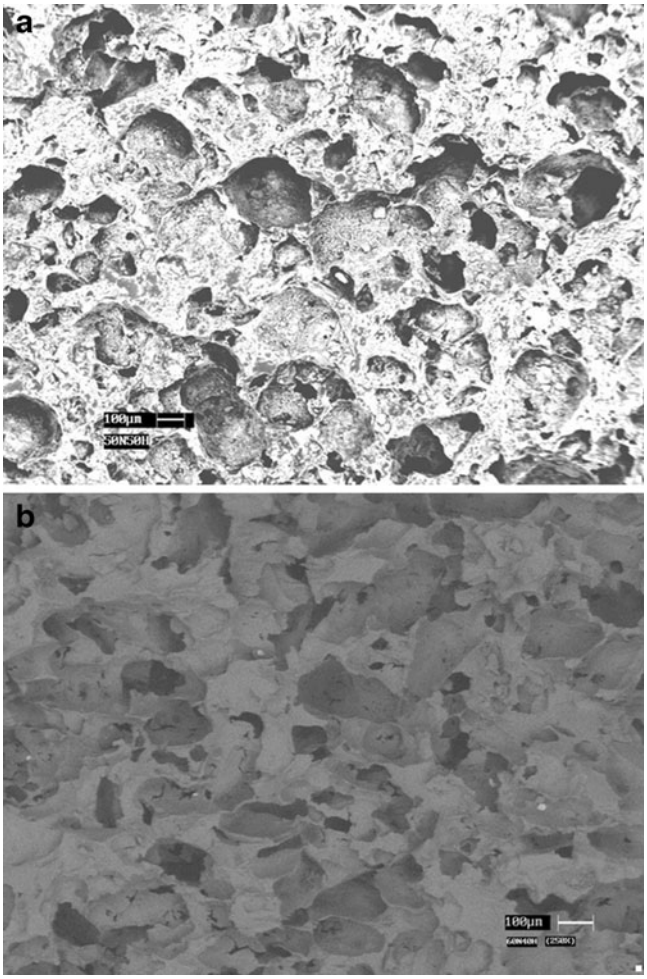

Fig. 3 SEM micrograph of the (**a**) 50N50H (**b**) 60N40H sample.

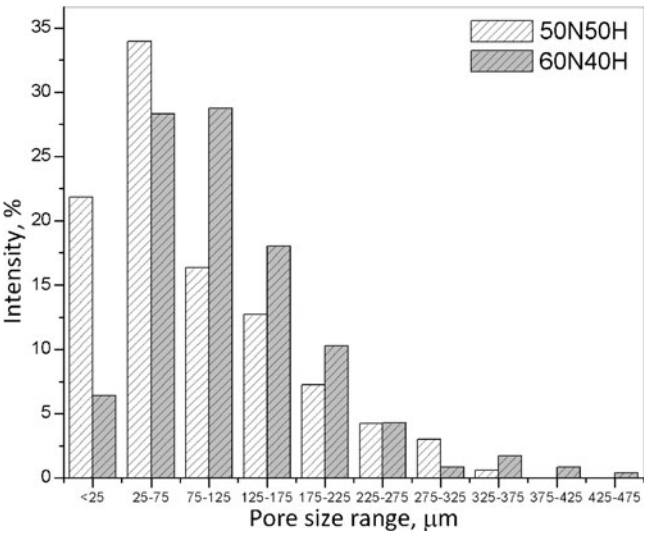

Fig. 4 Histogram to show the pore size distribution obtained from the image analysis of microstructures for 50N50H and 60N40H samples.

connection of pores was found for all micrographs. Subsurface interconnections were found in the range from 30 to 120 μm throughout the microstructures of 60N40H samples and about 10–100 μm for 50N50H samples.

Characterization of Drug-Loaded Porous Scaffolds

Adsorption efficiency of the drug CFS for 50N50H and 60N40H samples were on an average found to be ~48 and 82% respectively. Adsorption efficiency increased with increase of pore percentage and distribution of pores. Due to increase of the surface area of the pores, the drug adsorption efficiency was also increased for 60N40H samples. Surface charge in terms of zeta potential for HAp (fired at 1,250°C) with varying pH is given in Table IV. HAp surface had a high negative potential throughout the observed pH spectrum and hence could safely be said that in the physiologic pH spectrum it will behave as anionic. Moreover, it is the surface charge, which also had a definite role for adsorption to the surface of porous HAp as well as the cohesion between drug CFS and calcium phosphate.

We have also studied the surface morphology of HAp scaffolds loaded with drug (Figs. 5 (I) and (II)). The SEM studies showed microstructure of crystalline HAp and its closest approximated drug at the interface infused into the pores. Cracks were visible at the drug surface only (marked with white arrow). Visually, the interface was not distinguishable; hence, corresponding EDAX obtained are given in Figs. 5a–c. EDAX were taken at the points A, B and C and crosschecked for compositional variation (if any) along the interface. At point A, there were elements like Ca (calcium), P (phosphorous) and O (oxygen) corresponding the HAp structure. Point B on the other hand showed the presence of elements like S (sulphur), Na (sodium), nitrogen (N) and carbon (C) with significant reduction of peak intensity of Ca, P and O. This indicated the prevalence of drug molecules (CFS).

In Vitro Drug Elution Study

Release profiles of the drugs CFT and SUL in PBS and SBF were plotted separately in Figs. 6a and b. On an

Table IV Variation of Surface Charge (Zeta Potential) with Varying pH

pH	Zeta potential, mV
3.81	−27.4
5.16	−38.8
6.48	−38.8
7.55	−37.9
9.67	−40.2

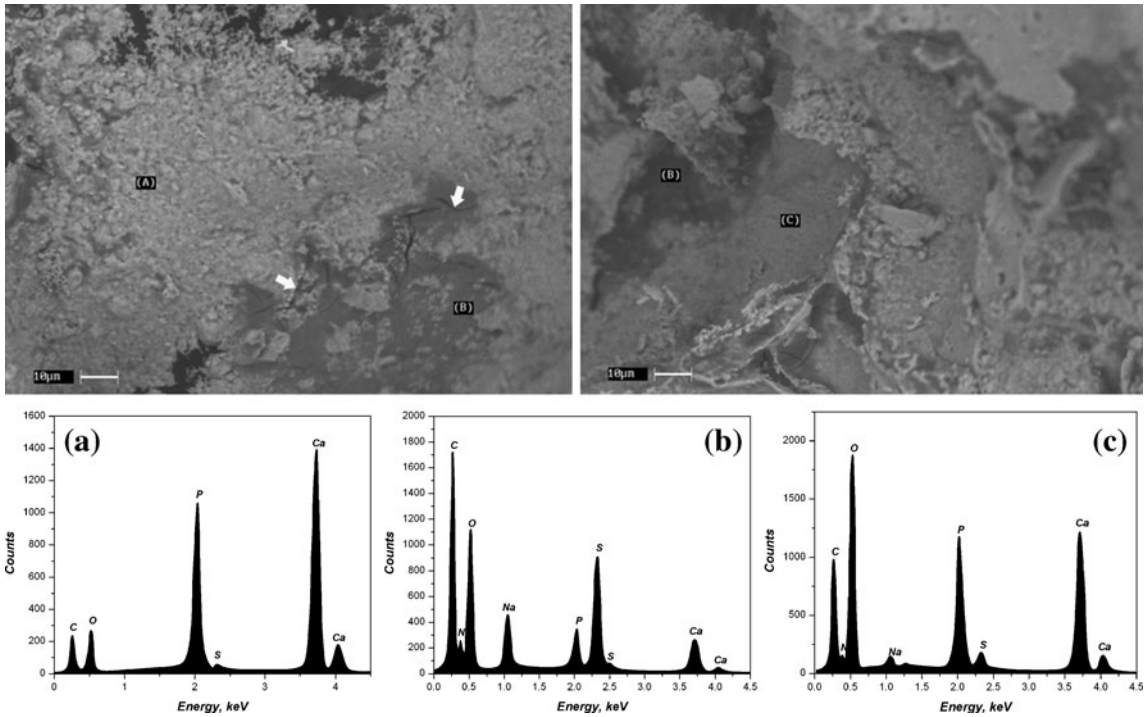

Fig. 5 (*I*) and (*II*). SEM photomicrograph of the 50N50H sample impregnated with the drug CFS. EDAX were taken at the points A, B and C [shown in (*a*), (*b*) and (*c*)].

average, percent yield of the drug (CFS) in contact with PBS was found to be ~90.8% and 98.9% for 50N50H and 60N40H samples, respectively. In general, there was a burst release observed from all the samples followed by a much-restricted release profile. There was ~0.98 and 1.02 mg/mL CFT and 0.11 and 0.12 mg/mL SUL burst release in the very first day for two kinds of samples; the rate was subsequently dropped down up to fourth day, and subsequently the release became very slow and continued up to 42 days. Faster drug release was observed for 60N40H samples owing to its high percent porosity, higher interconnected pore sizes and bimodal distribution of pores. On the other hand, in contact with SBF, slow releases of both drugs were observed for total study period (Fig. 6b) of 42 days. Average percent yield was found to be ~79.4 and 93.6% for 50N50H and 60N40H samples, respectively. There was higher burst release of the individual drugs in the first day (2.54 and 3.58 mg/mL CFT and 0.98 and 2.81 mg/mL SUL from 50N50H and 60N40H samples respectively) in contact with SBF, but the rate of release was very uniform until 42 days. After 42 days, higher CFS release was observed for 50N50H samples than 60N40H samples. PBS had less effect on the drug elution rate for all the samples than SBF. Although the adsorption efficiency was better in 60N40H samples, the elution rate was much faster throughout the study period for both PBS and SBF.

In Vivo Study

Histological Examination

Histological sections for all group of animals (viz. Group I, II and III) taken after different days of observation period are given as a 3×3 matrix in Fig. 7. In the present study, the histological section obtained on day 12 of group I revealed osteomyelitic changes characterized by degenerative changes of haemopoigenesis centre, degeneration of osteophytes, fat cells along with mild fibro vascular proliferation of connective tissues. Bone marrow in the peripheral region showed infiltration with mononuclear cells and osteoclasts. The histological features on days 21 and 42 were more intensified and aggressive in terms of osteomyelitic changes. The histological section on day 12 in group III showed mild calcification of the bony osteoid with normal laminar formation. Cellular reaction with osteoclasts and other infiltrating cells was predominant in between laminae. The section on day 21 showed a proliferative reaction with cellular integration and admixture of fibrous tissue and osteoid proliferation. The section on day 42

Fig. 6 **a** *In vitro* individual drug (ceftriaxone and sulbactam) elution profile of 50N50H and 60N40H samples in contact with PBS at pH 7.4 and temperature 37°C. **b** *In vitro* individual drug (ceftriaxone and sulbactam) elution profile of 50N50H and 60N40H samples in contact with SBF at pH 7.4 and temperature 37°C.

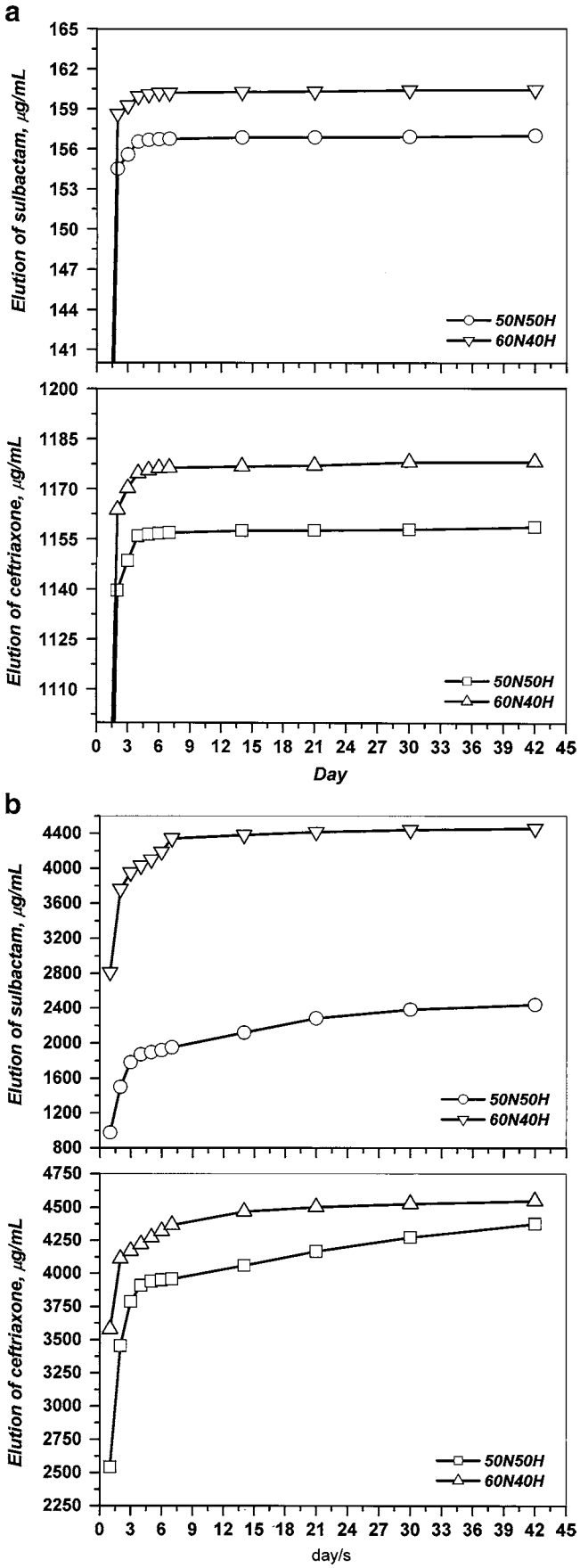

showed a zone of inflammatory cells hyperplasia encircled by delicate connective tissues. On the other hand, the sections taken on 12 days from group II showed fibro-purulent reaction with mucin deposit and presence of polymorphonuclear cells. Some portion of medulla was replaced by cellular clumps of mononuclear cells with eosinophilic exudation. This section was featured with chronic infection characterized by scanty vascularity of the cortico-medullary junction and presence of giant cells. The section of 21 days showed a degenerative stage of bony lamina with scanty cellular reaction and evidence of exudation with oedematous fluid. The other structures were indistinct. On day 42, the section revealed moderate parenchymal vascularity with formation of partial callus around the osteoid while the haversian system retained their structures.

Radiological Examination

In the present study, osteomyelitis was inducted successfully in animals of all groups by inoculating *Staphylococcus aureus* as evidenced by periosteal reaction and radio dense lamellated new bone formation. Lytic changes and thinning of bony cortex were evident. Prominent endosteal reaction with more radio dense bone marrow was visible. Both the osteophytic and lytic changes were suggestive of osteomyelitis (Fig. 8). In group II animals, the radiograph on 12 days showed increased radio-opacity along with loss of characteristics of cancellous bone in proximal metaphysis of tibia. Both the phytic and lytic changes were prominent in proximal metaphysis. Formation of new bone was of amorphous type. Moderate endosteal reaction was clearly visible. Anterior cortical border of proximal metaphysis of tibia showed discontinuation in some places, and epiphyseal cartilage showed secondary osteophytic changes (Fig. 9a). The radiograph on 21 days showed variable radio density in anterior border of proximal metaphysis along with discontinuation of cortex in few places. Endosteal reaction was mild. Reestablishment of the medullary cavity and remodelling of cortex were noticeable (Fig. 9b). On 42 days, the radiograph showed few radiolucent zones characteristic of osteoclastic changes. Absence of periosteal and endosteal reaction, reestablishment of medullary cavity along with cortical continuation as observed from the radiograph demonstrated the process of healing was still continuing and yet to complete (Fig. 9c).

In group III, day 12 radiographs showed unabsorbed circular, radio dense HAp block near the radiolucent zone of inoculum. Continuity of periosteum was nearly established with mild periosteal reaction. Osteoblastic activity in some places of proximal metaphysic of tibia was visible. Radio density of diaphysis and metaphysis were nearly similar. There was moderately controlled infection as evidenced by absence of sequestrum, and the remodelling

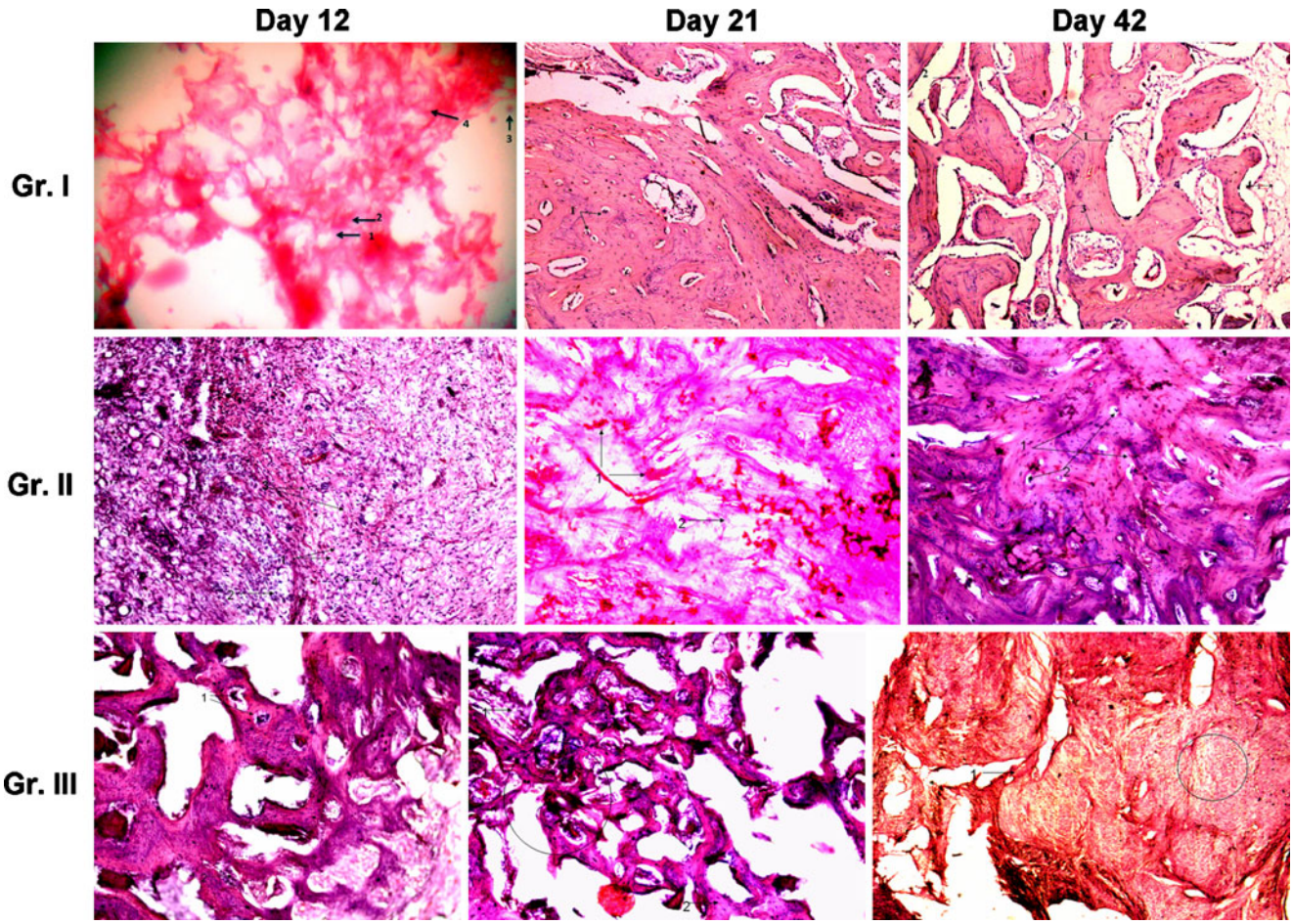

Fig. 7 3 × 3 matrix showing the histological sections for all three groups (viz. Group I, II and III) after different days of observation period (viz. 12, 21 and 42 days). R1 × C1: 1. Bony matrix 2. Osteocyte 3. Osteoclast 4. Immature bony osteoid. R1 × C2: Osteoblastic activity (1) in Haversian canal. In between canaliculi, there is infiltration with mononuclear cells and osteoclasts (2). Some portion of Haversian system showed discontinuity in relation to canalicular space due to supervening edema and cellular infiltration (3). R1 × C3: Vascular proliferation in and around Haversian canal and canalicular spaces (1). The thin wall blood vessel shows exudation with edema and mononuclear cells and scanty RBCs (2). In the middle of the section there are perivascular proliferations of mononuclear cells (3) and some vacuolation in the osteoblastic stroma (4) indicates acute phase of osteomyelitis. R2 × C1: Fibropurullent reaction with mucin deposit (1) and presence of polymorphonuclear cells (2). Some portion of medulla is replaced by cellular clumps of mononuclear cells with eosinophilic exudation (3). The vascularity of the corticomedullary junction is scanty indicating a persistent infection. The presence of giant cells (4) indicate the chronicity of the disease. R2 × C2: Degenerative stage of bony lamina (1) with scanty cellular reaction. In between laminae, there is also evidence of exudation with edematous fluid (2). The other structures are indistinct. R2 × C3: Formation of partial callus around the osteoid (1). The haversian system (2) retains their structures. Vascularity of the bony parenchyma is moderate (3). R3 × C1: Mild calcification of the bony osteoid (1). The laminar formation is normal. In between laminae, cellular reaction with osteoclast and other infiltrating cells are predominant (2). R3 × C2: Cellular integration, admixture of fibrous tissue (1) and osteoid (2) proliferation mimicking a proliferative reaction (*circle*). R3 × C3: Zone of cellular hyperplasia by inflammatory cells (*circle*), which is encircled by delicate connective tissue (1).

at the site of infection was ascertainable (Fig. 10a). The lateral radiograph on day 21 showed unaltered radio opaque circular antibiotic-impregnated HAp implant in proximal part of tibia. Continuation of periosteum, absence of sequestrum and similar diaphyseal and metaphyseal radio-opacity of medullary cavity clearly demonstrated early healing process. Characteristic appearance of metaphyseal spongy bone was also evident, and no periosteal reaction was radiographically demonstrated (Fig. 10b). Radiograph on 42 days showed moderately absorbed, nearly circular antibiotic-impregnated HAp block of similar radio density to that of cortex. Reestablishment of medullary cavity was prominent. Typical characteristic of metaphyseal bone is visible. Continuity of periosteum is established. No periosteal or endosteal reaction is radiographically evident. The radiographic feature is suggestive of repair or healed status of osteomyelitis (Fig. 10c).

Drug Concentration

It has been observed from Fig. 11a and b that there was an initial high release of CFS in HAp-implanted group (group III) as compared to group II in bone on day 12. The release of CFT in bone of HAp-implanted group is higher in the

Fig. 8 Radiograph of tibia-fibula. The osteophytic and lytic changes are suggestive of osteomyelitis (group I animals).

total study period as compared to concentration of SUL in the same group, which was nearly the same for the same period. There was a declining tendency of concentration of CFS on day 42 as compared to previous days of the same group as well as parenteral group. Concentration of CFS in serum of group III revealed initial slow release followed by increasing tendency on day 21 and 42, whereas, in group II, serum concentration of CFS showed initial higher value which remained nearly the same throughout the study period.

SEM of the Cortical Bone

Microstructures of bone defect sites for all the groups of animals are given in Figs. 12a–d. Figs. 12a and b display the status of bone after 42 days when no treatment was provided (Group I) after development of osteomyelitis (i.e. control) and the site when parenterally treated (Group II) by CFS, respectively. Figs. 12c and d portray the status of bone after 21 and 42 days when implanted with drug-loaded porous HAp implants (Group III). It was observed that after 42 days in group I, there was abundance of RBC cells together with decalcification of the bony matrix, indicative of osteolytic activity of the *S. aureus* at the control site. There was insignificant presence of bridging callus and fibro cartilaginous tissues at the centre of the defect, which indicates that mature bone cell formation was not completed after parenteral treatment of 42 days. On the other hand, drug-incorporated porous HAp sample showed reticulo formation of collagenous structure and penetration of bony trabeculae into the porous structure by 21 days and complete absence of any RBC cells, indicating faster bone mineralization with no reincarnation of the bacteria at the defect site. Vascularization by bony tissue and some immature bony sites were also noticed after 21 days. By 42 days, matured bone covered the defect site where regularly arranged osteons at the edge of the pores were noticed. Inside of such implant, there were still some abstract collagenous tissues, indicating bone mineralization process was still continuing at the inside.

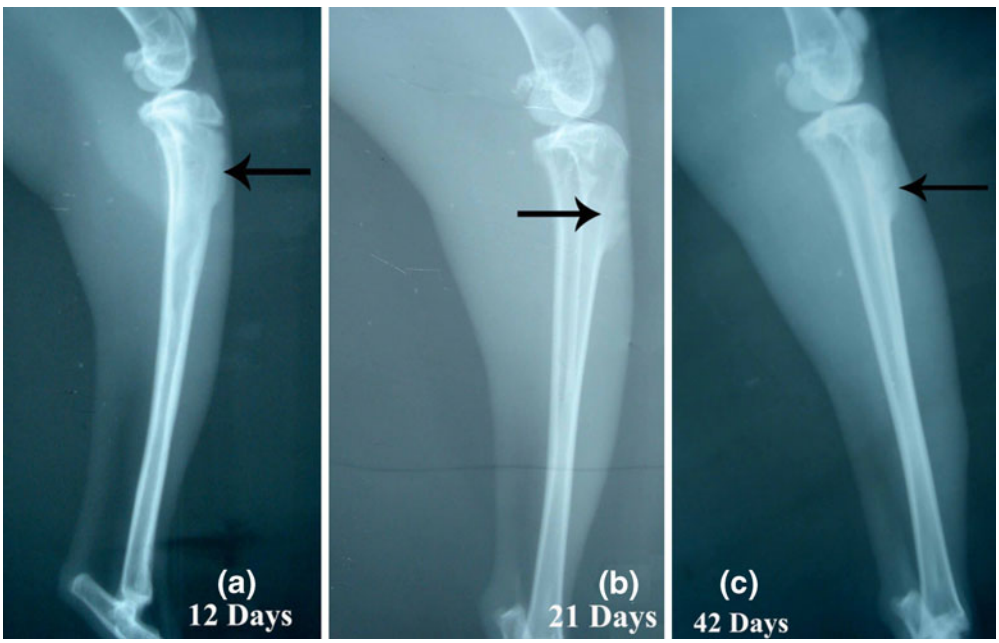

Fig. 9 Lateral radiograph of tibia-fibula taken for group II animals after (**a**) 12 days, (**b**) 21 days and (**c**) 42 days.

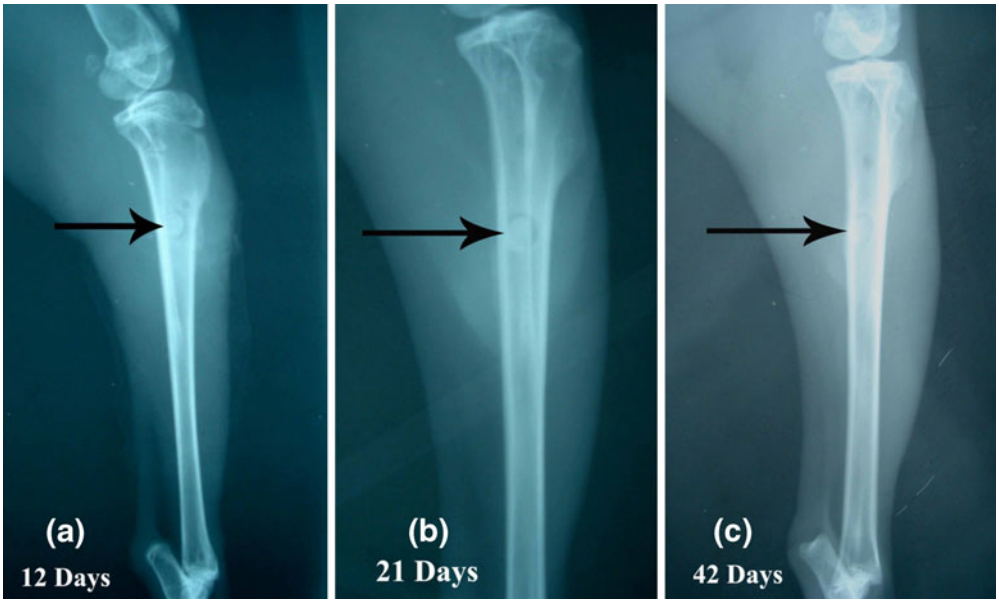

Fig. 10 Lateral radiograph of tibia-fibula taken for group III animals after (**a**) 12 days, (**b**) 21 days and (**c**) 42 days.

DISCUSSION

Because of its biocompatibility, bioactivity, rapid attachment of osteoblasts and non-requirement of follow-up surgery, HAp is considered a superior choice for drug carrier system and bioactive implant design than polymers (2,38,39). Several antibiotics together with porous HAp scaffold have been tried as delivery system to treat chronic osteomyelitis (40). Hitherto, to the best of our knowledge, this is the first report of comprehensive and integrated study that evaluates the impact of pore conditions (which includes pore percentage, size, morphology and most importantly interconnectivity and distribution of such pores), incorporating a rational antibiotic combination with an extensive six-week evaluation of *in vitro* drug release followed by a selection of desirable formulation that was further subjected to a six-week animal trial. The pore percentage level has been considered earlier only between 10% and 40% (41,42). Increasing the pore percentage further to 50 or 60 could provide results for better understanding and logical designing of porous HAp systems that could synergistically deliver drug and enhance bone formation. In the present study, we have tried to address the above concerns by varying the pore conditions and confirmed the elution rate (*in vitro* in contact with PBS and SBF) before going into the detailed animal trials.

Powder Characterization

The present method employed to synthesize HAp as well as its porous form by incorporating a fugitive material was a simple and economical method. The as-dried HAp powder and powders fired at 800°C and 1,250°C were subjected to XRD analysis to ascertain conditions like crystallinity and

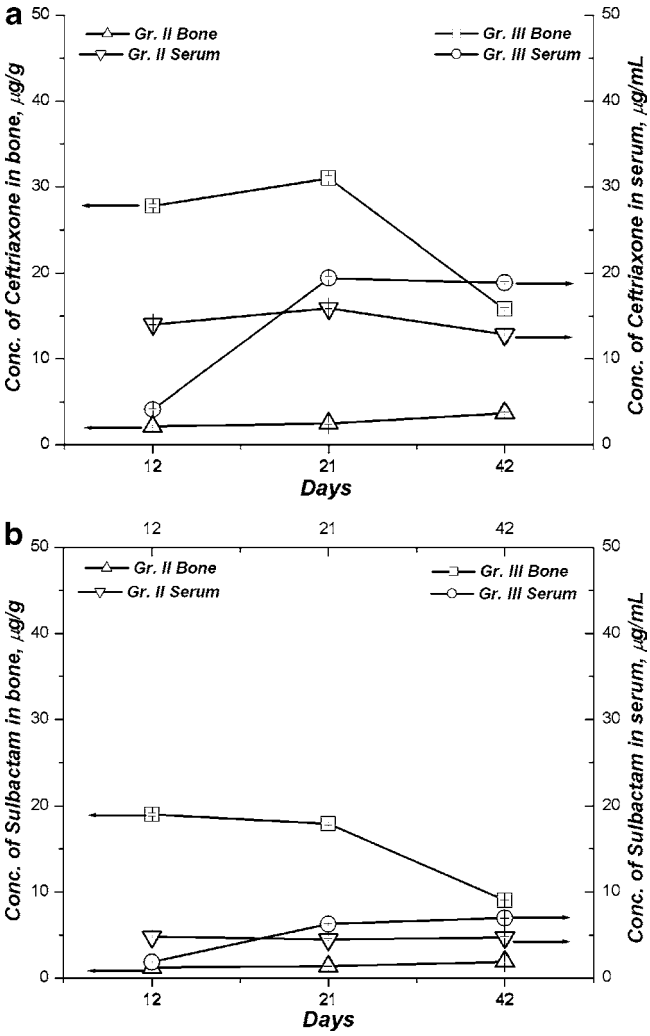

Fig. 11 *In vivo* concentration of (**a**) ceftriaxone and (**b**) Sulbactam in different groups over different days interval. [Group II = Parenteral injection of antibiotic; Group III = HAp implanted group].

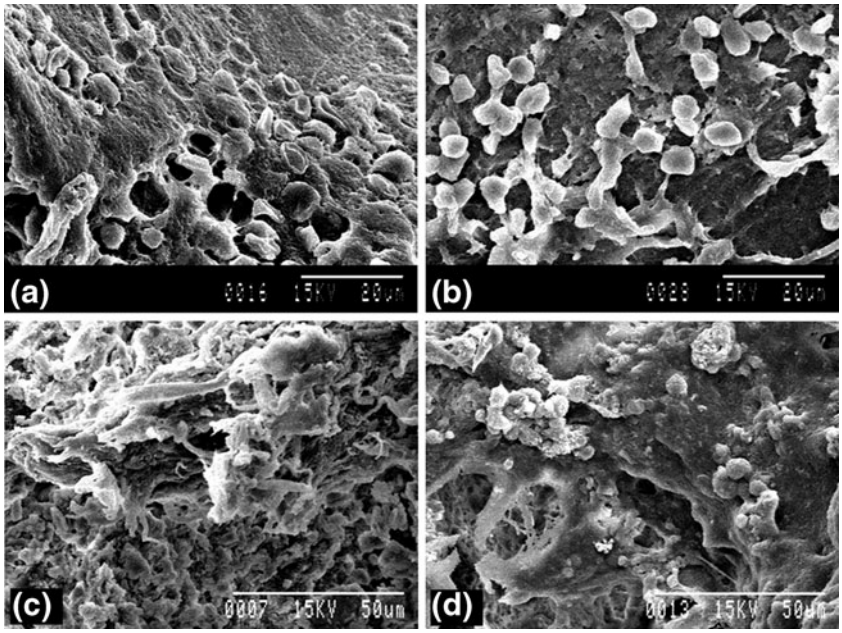

Fig. 12 SEM microstructures of bone defect sites for all groups of animals taken after: (**a**) 42 days for group I, (**b**) 42 days for group II, (**c**) 21 days for group III and (**d**) 42 days for group III.

powder morphology suitable for final applications. The other purpose was to ascertain phase changes and modifications, if any, when sintered finally. XRD studies revealed that the powders were composed of single phase of HAp with absence of any other phase even in minor quantity for all studied temperatures.

X_c, which gives an idea of presence of amorphous content in the material, can affect different physical, chemical and mechanical properties after sintering also. With increase of crystallinity, the degree of attachment of drug decreases. With the increase of crystallinity of our synthesized HAp powders to 98.3% at the selected sintering temperature, the degree of attachment of drugs may be expected to be low with the porous scaffold when sintered than as synthesized HAp powders.

The absence of band positions of OH^- at 3,580 and 630 cm^{-1} in the FT-IR spectrum for as-dried powders and their presence in those for powders dried at 800°C and 1,250°C indicate that the as-dried powders were calcium deficient HAp but got converted to HAp phase when fired at 800°C. Amorphous nature of formed apatite crystals was also inferred from the corresponding transmittance values of the band positions which again increased with the increasing temperature.

Another factor, which also contributes to drug adsorption, is the presence of some carbonate group into the HAp structure, which probably came from the impurity of the raw materials (43). It was also observed that the carbonate presence was not detected in the XRD pattern but in the FTIR spectrum (Fig. 2c). As dried powder was composed of amorphous or defective calcium phosphate which is usually expressed by the formula $Ca_{10-x}(PO_4)_{6-x}(HPO_4)_x(OH)_{2-x}$ (44). In fact, as-dried powder showed presence of this HPO_4^{2-} in minute quantity and retained at 800°C samples. This indicates that structural reorientation was occurring with the manifestation of thermal energy. In every FTIR spectrum, there was a peak (marked circle) around 2,362 cm^{-1} which came from the CO_2 of atmosphere and hence was ignored for subsequent interpretation processes. As for XRD and FTIR reports, they both showed there was no degradation of the HAp phase from as-dried state to the sintered stage.

Characterization of Porous and Drug-Loaded Scaffolds

Microstructure can also affect the adsorption and release behaviour both *in vitro* and *in vivo* (45). For example, open porosity is most important because it is related to properties such as permeability and surface area. A bimodal distribution of pores is thought to be ideal for HAp to be used for sustained release of drug to the bone which not only includes large pores (more than 50 μm) to allow bone ingrowth into the pores but also small pores to facilitate the slow release of drug (7). Most of the previous reports showed either the effect of low percentage of pores with presence of macropores that eluted drug very fast (46) or porous compacted granules which eluted drug in non-uniform rate; degradation of calcium phosphate was another concern (42,47).

Increase in naphthalene content in the formulation resulted in higher porosity and hence lesser bulk density of 60N40H as expected. There was bimodal distribution of both micro- and macro-pores in these samples, and there were more numbers of micro-pores in 50N50H samples. Due to the higher percentage of porosity and open pore surfaces in 60N40H, the adsorption efficiency of the drug

increased. The presence of lesser amount of micropores in 60N40H samples also favoured high drug impregnation efficiency. This was also an indirect evidence of the better interconnectivity of pores in these samples. Pore interconnectivity is another important factor (48,49) often overlooked before scaffold design. Interconnected pores influence more critically than pore size alone.

Another parameter which also influences the drug attachment behaviour as well as degree of adhesion to the pore surface is the surface charge. Surface charge of HAp in aqueous media plays a significant role for drug attachment to the ceramic. This parameter in terms of zeta potential was particularly used for assessment of deflocculation characteristics while fabricating the porous HAp scaffold (50). However, this parameter was never discussed for its effect on drug attachment to the pore surface of HAp scaffold. In our study, HAp surface in aqueous media at the physiological pH (7.4) had a very high negative zeta potential (~38 mV), which was another factor responsible for better drug adhesion characteristics as evidenced from the values of adsorption efficiency as well as microstructure observed of CFS-impregnated scaffolds. Recently, negative surface charges of HAp have been reported to influence apatite nucleation, rapid cell attachment and faster tissue ingrowth (51,52). With the high negative surface charges of the HAp scaffolds fabricated in this study in addition to drug attachment, accelerated mineral deposition, rapid cell attachment and faster tissue ingrowth could be expected.

CFS had many carboxylic groups which could form hydrogen bonds with the HAp surface; consequently, drug molecules are retained on the pore surface (53). During drug loading, cations of both materials (i.e. ceramic and drug) inter-diffused; consequently, EDAX showed small humps of the peaks corresponding to CFS in the microstructure of HAp and vice versa. There was no as-such interface between these two materials (i.e. ceramic and drug), and the EDAX at the interface showed mixture of above elements. One of the reasons for absence of interfacial gap between the drug and pore surface was due to electrostatic attraction between the functional groups of CFS and Ca^{2+} and PO_4^{3-}. Further, high adhesion strength and subsequent cracks on the drug surface were due to higher surface potential on HAp surface, which contributed such phenomenon.

In Vitro Drug Elution Study

From the drug point of view, factors such as size (54), solubility (55) and binding capacity (56) to the biomaterial play a crucial role in the release of drugs. To elaborate, it should be quiet obvious for smaller molecules to easily pass through the pores and reach out faster when compared to bulkier molecules. Accordingly, the first step is to design the ceramic with high porosity and tailored pore number, size, shape, distribution and connectivity. The design again depends on the drug to be confined and subsequently released on the chemical nature of the wall, to achieve a greater control of the chemical interaction between the HAp and drug. Hence, the drug molecule included into the bioceramic matrix has to be considered. In general, the size of drug molecules falls within the nanometre scale; consequently, every porous material showing pore sizes higher than a few nanometres is expected to host these drug molecules. In addition, the higher the solubility of drug, the faster and greater its release. While comparing the drugs co-loaded in our study, sulbactam is a much smaller molecule than ceftriaxone with a molecular mass of 255.22 and 661.6, respectively. Sulbactam is readily soluble, and ceftriaxone is freely soluble in water. In accordance with the generalizations, it should be quite natural to expect a faster release of SUL and the same observed in PBS.

More elaborate release profiles were observed for 50N50H samples up to the total observation period. This was due to the prevalence of comparatively higher amount of micro-pores in these samples. 60N40H samples had more numbers and sizes of macropores, which caused much faster diffusion of the attached drug *in vitro* in both PBS and SBF. According to Vallet-Regí *et al.*, for drugs to be placed into pores, a material with homogeneous ordered pore distribution should be specially designed (53). In such material, the drug adsorption and subsequent delivery will be more regular and reproducible than that coming from a disordered pore distribution. In the present study, we observed that more numbers of interconnected pores played a vital role more than the homogeneity of the pores. Homogeneity is more important for mesoporous solids than its interconnectivity for both binding and release of the drug *in vitro*. However, the binding capacity of the drug to the biomaterial is an important factor to retard the drug release. The –COOH groups present in the drug molecule are primarily responsible for binding with ceramic biomaterials and the intensity of binding increases with the number of available carboxyl groups (57). Both the studied drugs have just one carboxyl group available. Hence, slower release of drug CFT could be due to 1) some other functional groups present in the CFT, which could have interacted to the HAp surface than that of SUL and 2) higher molecular weight and longer molecular chain than S.

SBF is an acellular fluid having inorganic ion concentrations similar (more than the composition of PBS) to those of human extra-cellular fluid, mainly used to reproduce formation of apatite on bioactive materials *in vitro*. Since SBF composition is almost similar to our body physiological fluids in terms of its composition of ions, we expected release profiles of drugs obtained from SBF-soaked samples to be a more accurate prediction of the *in vivo* situation.

These supersaturated solutions in contact with bioactive materials form a layer of HAp covering the substrate with due course of time depending on the conditions of test, bioactive material subjected and composition of SBF selected. In the present investigation, more slow and continuous release of the drugs was observed in SBF than with PBS, most probably due to formation of such layer which subsequently retarded the diffusion of drug molecule. The more pronounced burst release of drugs in PBS than SBF may also be attributed to the above stated reason. Similar observation was also noticed by Rai *et al.* (58), who demonstrated that SBF-soaked composites of polycaprolactone-tricalcium phosphate had delayed release of biomolecules and absence of total release in the total study period. Influences of other parameters, however, could be the same as explained earlier.

As to drug release mechanism, in general, the drug release pattern from porous HAp has been reported to be controlled by diffusion than matrix degradation (45,59). In our case, 50N50H samples might have followed the same kinetics but in SBF, while 60N40H samples most probably degraded on comparison to 50N50H along with its drug elution in both PBS and SBF due to its high amount, size and prevalence of macro-pores over micro-pores. Finally, from the above observations we had selected the 50N50H samples for further animal trial owing to its 50–55% porosity with an average pore size ~110 μm, having higher interconnectivity (10–100 μm), moderately high CFS adsorption efficiency (~50%) and finally with much slower, prolonged and homogeneous elution profile up to 42 days (higher than the MIC values) in contact with SBF.

In Vivo Study

Histological Examination

Among the animal trial results, histological findings remained one of the most important tools for detection of implant-host bone reaction and details of healing. The best proof of the efficiency of treatment of osteomyelitis could be observed in histopathological and microbiological findings (60). In the histological analysis, the trend of intramedullary new bone formation as well as curing of infection were higher in HAp-treated group as compared to parenteral-treated and control groups. Previous findings on biodegradable implants demonstrated that infection subsided by 3 weeks to 6 weeks, and inflammatory cells were replaced with bone-forming cells upon treatment of osteomyelitis (43,44,61). In this study, there was only a minimal reaction towards biomaterial and gradual new bone formation in the area, which suggest the acceptability of the implant as well as effective delivery of the antibiotic to osteomyelitic bone. Antibiotic-impregnated HAp group showed better osteoid proliferation and cellular infiltration with no periosteal reaction in and around the osteomyelitis area as compared to parenteral and control group, which clearly demonstrated a superior delivery system.

Radiological Examination

Radiological findings also showed development of osteomyelitis from initial bacterial colonization, which was progressing with inflammation and hyperaemia, ultimately led to formation of abscess. The abscess thus formed expands further, producing purulent exudates that enter and spread to the cortical bone via haversian and Volkmann's canals and ultimately lead to necrosis of fragments of bone sequestrum and lyses (62). The efficacy of systemically applied antibiotic (Group II) for precluding osteomyelitis seems to be very poor due to inability of this antibiotic to attain desirable concentration at the target site due to pathological conditions and blood-bone barrier (2). In Group III, newly grown periosteal bone was predominant, suggesting bone healing and remodeling, which are indicative of the infection being controlled with desired level of antibiotic concentration at the site and the implant material supporting reconstruction.

Drug Concentration

Finally, in the present study, the reason for the efficacy of CFS-loaded porous HAp scaffolds in the treatment of osteomyelitis is probably the advantageous pharmacokinetics at the site of infection. The pharmacokinetics of the combination drugs *in vivo* showed that therapeutic concentration, of antibiotic was maintained at the site of implantation, which was adequate to provide antimicrobial activity and always well above the minimum inhibitory concentration (MIC) of CFS against *Staphylococcus aureus*, which is 1 μg/mL (63).

The MIC of ceftriaxone depends on type of microorganisms. It has been reported that MIC of ceftriaxone varies between 1 and 10 μg/mL, which will affect the majority of susceptible microorganisms. In this study, MIC was maintained throughout the observation period in both *in vitro* and *in vivo*.

AUC of ceftriaxone in serum and bone after parenteral injection were 575.70 μg day/mL and 105.13 μg day/g, while the values were 482.41 μg day/mL and 1,153.54 μg day/g after implantation. On the other hand, AUC for sulbactum was 194.97 μg day/mL in serum and 58.48 μg day/g in bone following parenteral injection, while the said AUCs were 196.62 μg day/mL and 730.61 μg day/g in serum and bone after implantation in bone.

The serum concentration of drug exposure for group III exceeds group II, suggesting sustained release of drug at the

local site (bone) compared to parenteral injection. It is obvious that the concentration of drug will be decreased rapidly after parenteral injection (high concentration at a time), which might be due to elimination of drug from the body.

SEM of the Cortical Bone

From the SEM study of the bone-biomaterial interface of all groups it was found that group III animals had far better bone ingrowth into the deep pores through the inter-pore connections after 21 days, which became matured at day 42. Our findings also corroborated the findings of Tamai *et al.*, who showed that porous HAp with average interconnecting pores ~40 μm in diameter had bone in-growth into the deep pores (64). Intra-implant vascularization for group III animals' cortical sites after 21 days had a favourable gradient for draining out of the drug CFS through capillary of the bone tissue, which was occurring even after 42 days; meanwhile, the new bone on the surface became matured, and there was sign of further bone mineralization process subsurface. This finding also corroborated the findings of Castro *et al.* (65).

CONCLUSION

In the present investigation, a novel and rational approach was made to combine drugs including an irreversible β-lactamase inhibitor with β-lactam antibiotic with HAp ceramic matrix, which can deliver the drug locally and in a sustained fashion. Porous HAp scaffolds exhibiting two kinds of pore percentage with similar distribution of pores sizes have been studied in detail to cure osteomyelitis in animal model. It was established that lower pore percentage with a distribution of mainly micro-pores were found to be superior over the higher pore percentage both *in vitro* and *in vivo*. The criteria was matched with the 50N50H samples, which had 50–55% porosity with an average pore size ~110 μm, having higher interconnectivity (10–100 μm), moderately high adsorption efficiency (~50%) when loaded with CFS. CFS release from HAp implants was faster in PBS than SBF. Further, both the results of *in vitro* and *in vivo* drug elution after 42 days showed release higher than minimum inhibitory concentration of CFS against *Staphylococcus aureus*. *In vivo* studies also proved the superiority of CFS-loaded HAp implants than parenteral group based on eradication of infection and new bone formation.

Hence, it could be concluded that HAp-based porous scaffold loaded with CFS and designed porosity (in terms of micro- and macro-porosity, interconnectivity) was found to be an ideal delivery system which could locally and sustainably release the composite antibiotic in a reliable manner both in terms of *in vitro* drug elution behaviour in contact with SBF and *in vivo* animal trial. Conditions employed with the said drugs for their anchoring on porous HAp have been established depending on the drug chemistry. The chemical nature of porous HAp surface modulated the confinement and delivery kinetics of the drug that is the consequences of results of both *in vitro* and *in vivo* experiments.

ACKNOWLEDGEMENTS

The authors wish to express their sincere thanks for the financial support by Department of Science and Technology, India [T.1 (7)/TIFA/2006-CGCRI] and the Director, CGCRI, India and Vice Chancellor, West Bengal University of Animal and Fishery Sciences, Kolkata, India for their generous and kind support to this work. All the personnel related to the characterization of the materials are sincerely acknowledged.

REFERENCES

1. Nandi SK, Mukherjee P, Roy S, Kundu B, De DK, Basu D. Local antibiotic delivery systems for the treatment of osteomyelitis—a review. Mater Sci Engg C. 2009;29:2478–85.
2. Soundrapandian C, Datta S, Sa B. Drug-eluting implants for osteomyelitis. Crit Rev Ther Drug Carrier Syst. 2007;24:493–545.
3. Rao N, Lipsky BA. Optimising antimicrobial therapy in diabetic foot infections. Drugs. 2007;67:195–214.
4. Conterno LO, da Silva Filho CR. Antibiotics for treating chronic osteomyelitis in adults. Cochrane Database Syst Rev:CD004439 (2009).
5. Houghton TJ, Tanaka KS, Kang T, Dietrich E, Lafontaine Y, Delorme D *et al.* Linking bisphosphonates to the free amino groups in fluoroquinolones: preparation of osteotropic prodrugs for the prevention of osteomyelitis. J Med Chem. 2008;51:6955–69.
6. Soundrapandian C, Sa B, Datta S. Organic–inorganic composites for bone drug delivery. AAPS PharmSciTech (2009).
7. Walenkamp GH, Kleijn LL, de Leeuw M. Osteomyelitis treated with gentamicin-PMMA beads: 100 patients followed for 1–12 years. Acta Orthop Scand. 1998;69:518–22.
8. Neut D, van de Belt H, van Horn JR, van der Mei HC, Busscher HJ. Residual gentamicin-release from antibiotic-loaded polymethylmethacrylate beads after 5 years of implantation. Biomaterials. 2003;24:1829–31.
9. Kilian O, Hossain H, Flesch I, Sommer U, Nolting H, Chakraborty T *et al.* Elution kinetics, antimicrobial efficacy, and degradation and microvasculature of a new gentamicin-loaded collagen fleece. J Biomed Mater Res B Appl Biomater. 2009;90:210–22.
10. Colilla M, Manzano M, Vallet-Regi M. Recent advances in ceramic implants as drug delivery systems for biomedical applications. Int J Nanomedicine. 2008;3:403–14.
11. Nandi SK, Kundu B, Ghosh SK, Mandal TK, Datta S, De DK *et al.* Cefuroxime-impregnated calcium phosphates as an implantable delivery system in experimental osteomyelitis. Ceram Int. 2009;35:1367–76.
12. Bose S, Saha SK. Synthesis and characterization of hydroxyapatite nanopowders by emulsion technique. Chem Mater. 2003;15:4464–9.

13. Wu Y, Bose S. Nanocrystalline hydroxyapatite: micelle templated synthesis and characterization. Langmuir. 2005;21:3232–4.
14. Palmer LC, Newcomb CJ, Kaltz SR, Spoerke ED, Stupp SI. Biomimetic systems for hydroxyapatite mineralization inspired by bone and enamel. Chem Rev. 2008;108:4754–83.
15. Al-Sokanee ZN, Toabi AA, Al-Assadi MJ, Alassadi EA. The drug release study of ceftriaxone from porous hydroxyapatite scaffolds. AAPS PharmSciTech. 2009;10:772–9.
16. Bose S, Banerjee A, Dasgupta S, Bandyopadhyay A. Synthesis, processing, mechanical and biological property characterization of hydroxyapatite whisker-reinforced hydroxyapatite composites. J Am Ceram Soc. 2009;92:323–30.
17. Sedrakyan S, Zhou ZY, Perin L, Leach K, Mooney D, Kim TH. Tissue engineering of a small hand phalanx with a porously casted polylactic acid-polyglycolic acid copolymer. Tissue Eng. 2006;12:2675–83.
18. Yoshikawa H, Tamai N, Murase T, Myoui A. Interconnected porous hydroxyapatite ceramics for bone tissue engineering. J R Soc Interface. 2009;6 Suppl 3:S341–348.
19. Xue W, Bandyopadhyay A, Bose S. Polycaprolactone coated porous tricalcium phosphate scaffolds for controlled release of protein for tissue engineering. J Biomed Mater Res Part B Appl Biomater. 2009;91:831–8.
20. Xue W, Bandyopadhyay A, Bose S. Mesoporous calcium silicate for controlled release of bovine serum albumin protein. Acta Biomater. 2009;5:1686–96.
21. Mastrogiacomo M, Scaglione S, Martinetti R, Dolcini L, Beltrame F, Cancedda R *et al.* Role of scaffold internal structure on *in vivo* bone formation in macroporous calcium phosphate bioceramics. Biomaterials. 2006;27:3230–7.
22. Turco G, Marsich E, Bellomo F, Semeraro S, Donati I, Brun F *et al.* Alginate/Hydroxyapatite biocomposite for bone ingrowth: a trabecular structure with high and isotropic connectivity. Biomacromolecules. 2009;10:1575–83.
23. Oudadesse H, Derrien AC, Lucas-Girot A. Statistical experimental design for studies of porosity and compressive strength in composite materials applied as biomaterials. Eur Phys J Appl Phys. 2005;31:217–23.
24. Chanda A, Singha Oy R, Xue W, Bose S, Bandyopadhyay A. Bone cell-materials interaction on alumina ceramics with different grain sizes. Mater Sci Engg C. 2009;29:1201–6.
25. Bush K, Mobashery S. How beta-lactamases have driven pharmaceutical drug discovery. From mechanistic knowledge to clinical circumvention. Adv Exp Med Biol. 1998;456:71–98.
26. Bush K. The impact of beta-lactamases on the development of novel antimicrobial agents. Curr Opin Investig Drugs. 2002;3:1284–90.
27. Caron F, Gutmann L, Bure A, Pangon B, Vallois JM, Pechinot A *et al.* Ceftriaxone-sulbactam combination in rabbit endocarditis caused by a strain of Klebsiella pneumoniae producing extended-broad-spectrum TEM-3 beta-lactamase. Antimicrob Agents Chemother. 1990;34:2070–4.
28. Foulds G, Stankewich JP, Marshall DC, O'Brien MM, Hayes SL, Weidler DJ *et al.* Pharmacokinetics of sulbactam in humans. Antimicrob Agents Chemother. 1983;23:692–9.
29. Sinha MK, Sen PS, Basu D, Chattopadhyay S, Basu MK. An improved process for the synthesis of hydroxyapatite powder useful for biomedical applications. In CGCRI (ed.), India, 1998.
30. Landi E, Tampieri A, Celotti G, Sprio S. Densification behaviour and mechanisms of synthetic hydroxyapatites. J Eur Ceram Soc. 2000;20:2377–87.
31. D. Basuand M.K. Sinha. A process for the production of improved porous ocular implants and improved porous ocular implants produced thereby. In CGCRI (ed.), India, 2006.
32. Kokubo T, Kushitani H, Sakka S, Kitsugi T, Yamamuro T. Solutions able to reproduce *in vivo* surface-structure changes in bioactive glass-ceramic A-W. J Biomed Mater Res. 1990;24:721–34.
33. Norden CW. Experimental osteomyelitis. I. A description of the model. J Infect Dis. 1970;122:410–8.
34. Weng W, Baptista JL. Sol-gel derived porous hydroxyapatite coatings. J Mater Sci. 1998;9:159–63.
35. Choi D, Marra KG, Kumta PN. Chemical synthesis of hydroxyapatite/poly(e-caprolactone) composites. Mater Res Bull. 2004;39:417–32.
36. Narasaraju TSB, Phebe DE. Some physico-chemical aspects of hydroxylapatite. J Mater Sci. 1996;31:1–21.
37. Suetsugu Y, Shimoya I, Tanaka J. Configuration of carbonate ions in apatite structure determined by polarized infrared spectroscopy. J Am Ceram Soc. 1998;81:746–8.
38. Rokusek D, Davitt C, Bandyopadhyay A, Bose S, Hosick HL. Interaction of human osteoblasts with bioinert and bioactive ceramic substrates. J Biomed Mater Res. 2005;75:588–94.
39. Banerjee A, Bandyopadhyay A, Bose S. Hydroxyapatite nanopowders: synthesis, densification and cell-materials interaction. Mater Sci Engg C. 2007;27:729–35.
40. Ginebra MP, Traykova T, Planell JA. Calcium phosphate cements as bone drug delivery systems: a review. J Control Release. 2006;113:102–10.
41. Krajewski A, Ravaglioli A, Roncari E, Pinasco P, Montanari L. Porous ceramic bodies for drug delivery. J Mater Sci. 2000;11:763–71.
42. Hasegawa M, Sudo A, Komlev VS, Barinov SM, Uchida A. High release of antibiotic from a novel hydroxyapatite with bimodal pore size distribution. J Biomed Mater Res B Appl Biomater. 2004;70:332–9.
43. Sanchez E, Baro M, Soriano I, Perera A, Evora C. *In vivo–in vitro* study of biodegradable and osteointegrable gentamicin bone implants. Eur J Pharm Biopharm. 2001;52:151–8.
44. Tampieri A, Celotti G, Sprio S, Mingazzini C. Characteristics of synthetic hydroxyapatites and attempts to improve their thermal stability. Mater Chem Phys. 2000;64:54–61.
45. Netz DJ, Sepulveda P, Pandolfelli VC, Spadaro AC, Alencastre JB, Bentley MV *et al.* Potential use of gelcasting hydroxyapatite porous ceramic as an implantable drug delivery system. Int J Pharm. 2001;213:117–25.
46. Itokazu M, Yang W, Aoki T, Ohara A, Kato N. Synthesis of antibiotic-loaded interporous hydroxyapatite blocks by vacuum method and *in vitro* drug release testing. Biomaterials. 1998;19:817–9.
47. Pham HH, Luo P, Genin F, Dash AK. Synthesis and characterization of hydroxyapatite-ciprofloxacin delivery systems by precipitation and spray drying technique. AAPS PharmSciTech. 2002;3:E1.
48. Eggli PS, Muller W, Schenk RK. Porous hydroxyapatite and tricalcium phosphate cylinders with two different pore size ranges implanted in the cancellous bone of rabbits. A comparative histomorphometric and histologic study of bony ingrowth and implant substitution. Clin Orthop Relat Res. 1988;232:127–38.
49. Kuhne JH, Bartl R, Frisch B, Hammer C, Jansson V, Zimmer M. Bone formation in coralline hydroxyapatite. Effects of pore size studied in rabbits. Acta Orthop Scand. 1994;65:246–52.
50. Rodriguez-Lorenzo LM, Vallet-Regi M, Ferreira JM. Colloidal processing of hydroxyapatite. Biomaterials. 2001;22:1847–52.
51. Bodhak S, Bose S, Bandyopadhyay A. Role of surface charge and wettability on early stage mineralization and bone cell-materials interactions of polarized hydroxyapatite. Acta Biomater. 2009;5:2178–88.
52. Bodhak S, Bose S, Bandyopadhyay A. Electrically polarized HAp-coated Ti: *in vitro* bone cell–material interactions. Acta Biomater. 2010;6:641–51.

53. Vallet-Regi M, Balas F, Colilla M, Manzano M. Drug confinement and delivery in ceramic implants. Drug Metab Lett. 2007;1:37–40.
54. Vallet-Regí M, Ruiz-González L, Izquierdo-Barba I, González-Calbet JM. Revisiting silica based ordered mesoporous materials: medical applications. J Mater Chem. 2006;16:26–31.
55. Lebugle A, Rodrigues A, Bonnevialle P, Voigt JJ, Canal P, Rodriguez F. Study of implantable calcium phosphate systems for the slow release of methotrexate. Biomaterials. 2002;23:3517–22.
56. Burgos AE, Belchior JC, Sinisterra RD. Controlled release of rhodium (II) carboxylates and their association complexes with cyclodextrins from hydroxyapatite matrix. Biomaterials. 2002;23:2519–26.
57. Stigter M, Bezemer J, de Groot K, Layrolle P. Incorporation of different antibiotics into carbonated hydroxyapatite coatings on titanium implants, release and antibiotic efficacy. J Control Release. 2004;99:127–37.
58. Rai B, Teoh SH, Ho KH. An *in vitro* evaluation of PCL-TCP composites as delivery systems for platelet-rich plasma. J Control Release. 2005;107:330–42.
59. Higuchi T. Mechanism of sustained-action medication. Theoretical analysis of rate of release of solid drugs dispersed in solid matrices. J Pharm Sci. 1963;52:1145–9.
60. Joosten U, Joist A, Frebel T, Brandt B, Diederichs S, von Eiff C. Evaluation of an *in situ* setting injectable calcium phosphate as a new carrier material for gentamicin in the treatment of chronic osteomyelitis: studies *in vitro* and *in vivo*. Biomaterials. 2004;25:4287–95.
61. Korkusuz F, Korkusuz P, Eksioglu F, Gursel I, Hasirci V. *In vivo* response to biodegradable controlled antibiotic release systems. J Biomed Mater Res. 2001;55:217–28.
62. Girschick HJ, Zimmer C, Klaus G, Darge K, Dick A, Morbach H. Chronic recurrent multifocal osteomyelitis: what is it and how should it be treated? Nat Clin Pract. 2007;3:733–8.
63. Shrivastava SM, Saurabh S, Rai D, Dwivedi VK, Chaudhary M. *In vitro* microbial efficacy of sulbactomax: a novel fixed dose combination of ceftriaxone sulbactam and ceftriaxone alone. Curr Drug Ther. 2009;4:73–7.
64. Tamai N, Myoui A, Tomita T, Nakase T, Tanaka J, Ochi T *et al.* Novel hydroxyapatite ceramics with an interconnective porous structure exhibit superior osteoconduction *in vivo*. J Biomed Mater Res. 2002;59:110–7.
65. Castro C, Sanchez E, Delgado A, Soriano I, Nunez P, Baro M *et al.* Ciprofloxacin implants for bone infection. *In vitro–in vivo* characterization. J Control Release. 2003;93:341–54.